Nanoscale Advances

ROYAL SOCIETY OF CHEMISTRY

PAPER

View Article Online
View Journal | View Issue

Cite this: *Nanoscale Adv.*, 2021, **3**, 3136

Ion shuttling between emulsion droplets by crown ether modified gold nanoparticles†

Casper Kunstmann-Olsen, ‡*[a] Domagoj Belić, [a] Dan F. Bradley, [a] Stephen P. Danks, [a] Yuri A. Diaz Fernandez, [b] Marcin P. Grzelczak, [a] Alexander P. Hill,[a] Xiaohang Qiao, [a] Rasmita Raval,[a] Ioritz Sorzabal-Bellido [b] and Mathias Brust *[a]

Received 4th January 2021
Accepted 9th April 2021

DOI: 10.1039/d1na00009h

rsc.li/nanoscale-advances

Selective unidirectional transport of barium ions between droplets in a water-in-chloroform emulsion is demonstrated. Gold nanoparticles (GNPs) modified with a thiolated crown ether act as barium ion complexing shuttles that carry the ions from one population of droplets (*source*) to another (*target*). This process is driven by a steep barium ion concentration gradient between *source* and *target* droplets. The concentration of barium ions in the target droplets is kept low at all times by the precipitation of insoluble barium sulfate. A potential role of electrostatically coupled secondary processes that maintain the electroneutrality of the emulsion droplets is discussed. Charging of the GNP metal cores by electron transfer in the presence of the Fe(II)/Fe(III) redox couple appears to affect the partitioning of the GNPs between the water droplets and the chloroform phase. Processes have been monitored and studied by optical microscopy, Raman spectroscopy, cryogenic scanning electron microscopy (cryo-SEM) and zeta potential. The shuttle action of the GNPs has further been demonstrated electrochemically in a model system.

Introduction

In living cells, the energy carrier ATP is formed by mechanistically coupling a downhill flux of ions with the uphill phosphorylation of ADP. The driving force is the steep proton concentration gradient across the inner mitochondrial membrane. Such molecular scale processes that are sustained far from chemical equilibrium are not limited to biological systems. Significant advances have been made in the creation of molecular motors and other machinery, where nanoscale motion is coupled to a spontaneous chemical reaction that provides the driving force.[1–16] The architectural and organizational sophistication of these supramolecular approaches notwithstanding, what matters conceptually is that the result can be viewed as a dynamic process rather than a static product. Hence, it is worthwhile to consider also very simple chemical reactions as a source of energy. Batteries and fuel cells are the most prominent examples of such systems, where a chemical reaction results in the flow of electric current. The reactants are kept apart in macroscopic containers to prevent decoupling from the generation of current by direct and uncontrolled electron transfer. This concept of trapping a reaction away from equilibrium by compartmentalization[10,11,17–23] is a principle batteries and biological systems have in common. On the microscopic scale, this represents a significant challenge, which living organisms meet by their cellular and subcellular organization. Here, we demonstrate the use of surfactant-stabilized emulsion droplets as microscale compartments that house reactive species and keep them apart from each other until a transport mechanism is provided, which allows the reaction to proceed. The precipitation of barium sulfate has been chosen as a simple model reaction as it can provide the system with a strong thermodynamic driving force and is readily monitored with minimum experimental effort. Ion transport between the emulsion droplets occurs *via* crown ether modified gold nanoparticles (GNPs) that complex barium ions and act as shuttles. Charge neutral transport of ion-pairs assisted by similar cation-complexing macrocycles is well established in phase transfer catalysis.[24]

Results and discussion

Two different water-in-chloroform emulsions were prepared by vigorously shaking a small volume of water with a larger one of chloroform in the presence of the nonionic surfactant Span80

[a]*University of Liverpool, Department of Chemistry, Crown Street, Liverpool L69 7ZD, UK. E-mail: mbrust@liverpool.ac.uk; casper.kunstmann@york.ac.uk*

[b]*University of Liverpool, Department of Chemistry, Open Innovation Hub for Antimicrobial Surfaces, Surface Science Research Centre, Liverpool L69 3BX, UK*

† Electronic supplementary information (ESI) available: Emulsion details, additional images of aqueous droplets with barium sulfate under various conditions and additional SEM images. Also, a video showing the formation of $BaSO_4$ precipitates in emulsion droplets, and discussions of control experiments and complexation equilibria. See DOI: 10.1039/d1na00009h

‡ Current address: University of York, Dep. Of Physics, Heslington, York, YO10 5DD, UK.

as standard stabilizer.[25] The emulsions formed opaque layers floating on top of the clear chloroform phases (Fig. ESI1†). This implies that the water/chloroform ratio within the emulsion layer is self-selected and cannot be adjusted at will. Inspection by optical microscopy revealed densely packed stable water droplets within a continuous chloroform matrix. The aqueous component of one emulsion contained barium chloride, and that of the other potassium sulfate and the fluorescent dye calcein as a label. Then, both emulsions were carefully combined, and samples were inspected by optical microscopy. Fig. 1a shows a typical micrograph of such a mixture (images obtained within 10 minutes of mixing). The two different populations of droplets can easily be distinguished by the presence of the dye in one of them. No changes were observed even after several days, and the droplet size distributions remained the same (Fig. ESI2†). This suggests that the different droplets do not merge or otherwise exchange significant portions of liquid.[26,27] Likewise, there is no indication of barium sulfate precipitation, neither by optical microscopy (Fig. 1a) nor in the Raman spectrum (Fig. 1b) of the emulsion confirming that there is no significant exchange of ions between the different droplets. The experiment was then repeated with adding either 4 or 7 nm gold nanoparticles (GNPs) modified with a barium ion complexing 18-crown-6-CH_2-SH ligand[28] to either of the aqueous phases before making the emulsions. Crown-ethers have been used before to functionalize nanoparticles of up to *ca.* 40 nm in size and to modulate their dispersibility and phase transfer between water and oil.[28–35] When shaking the emulsion, the chloroform sublayers immediately adopted a reddish brown (4 nm GNPs) or pink (7 nm GNPs) color, which we attribute to the transfer of some GNPs to the chloroform phase (see Fig. ESI1†). Note that the as prepared GNPs are not directly dispersible in chloroform and hence always had to be added to the aqueous phases before making the emulsions.

After combining the emulsions in the presence of GNPs, the immediate formation of a precipitate was now observed but limited strictly to the calcein-labelled droplets containing the sulfate (Fig. 1a *right*). See also the attached movie which shows the onset and progress of this precipitation (and additional micrographs of precipitation in droplets in Fig. ESI3 and ESI5†). These processes appear to reach completion after about 10 minutes. Longer observations of the systems (up to several days) show no further formation of precipitate, nor coalescence of droplets. Raman spectroscopy confirmed the presence of barium sulfate, which was also imaged by cryo-ESEM of emulsions (Fig. 1c). Apart from the barium sulfate peak, the Raman spectrum of the sample shows a few additional very small signals, which may be due to enhancement by the GNPs. Control experiments with crown ether alone or with GNPs not modified with crown ether (PEG stabilized) did not lead to the formation of a precipitate. We interpret our observations as the transport of barium ions by the crown ether modified GNPs from one type of droplets (*source*) to another (*target*) followed by precipitation as sulfate (Fig. 1d). Given the relatively low concentration of the GNPs in the nanomolar range, it can be inferred that they need to go back and forth between the

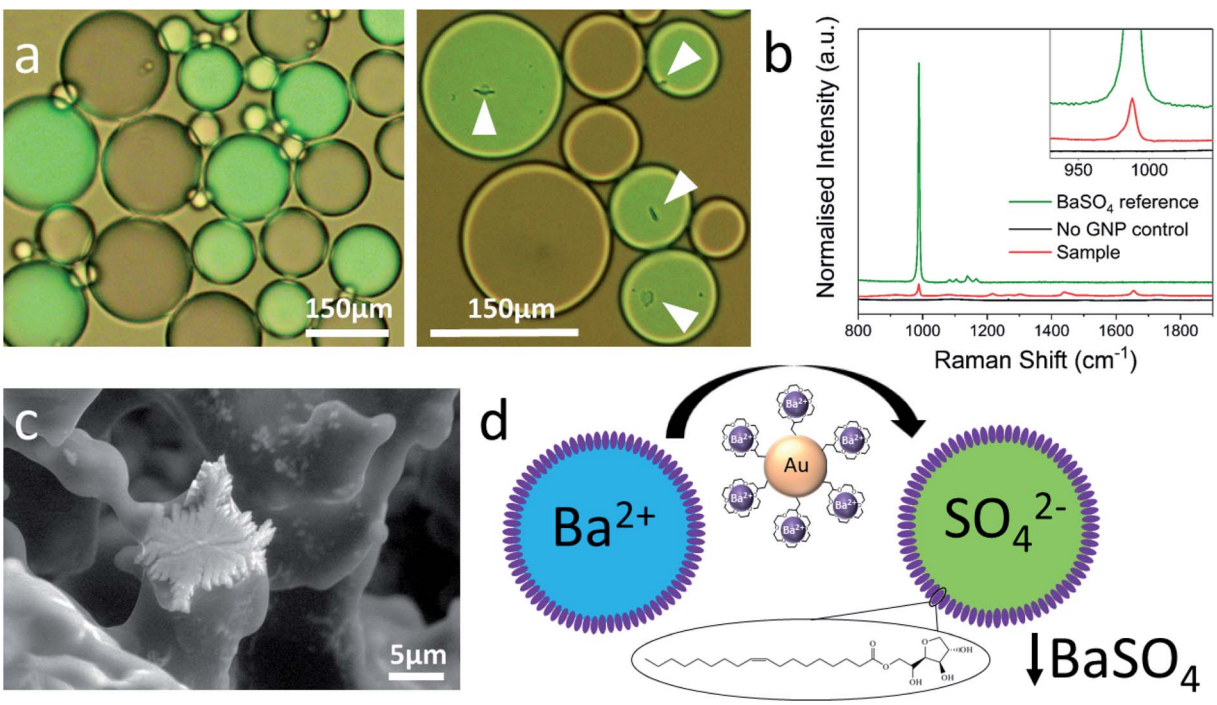

Fig. 1 (a) Optical micrographs of the emulsion in the absence of GNPs (left) and in their presence (right). White tags point at barium sulfate precipitates. Droplets containing sulfate are fluorescently labelled (green). Images were obtained within 10 minutes of mixing. (b) Raman microscopy confirms that the precipitate is $BaSO_4$ and that no detectable amount of it is formed in the absence of GNPs. (c) Cryo-ESEM image of $BaSO_4$ crystals at the surface of a shock-frozen emulsion droplet (see ESI6† for details and more images). (d) Schematic of GNP-mediated barium transport from a *source* droplet (blue) to a sulfate containing *target* droplet (green).

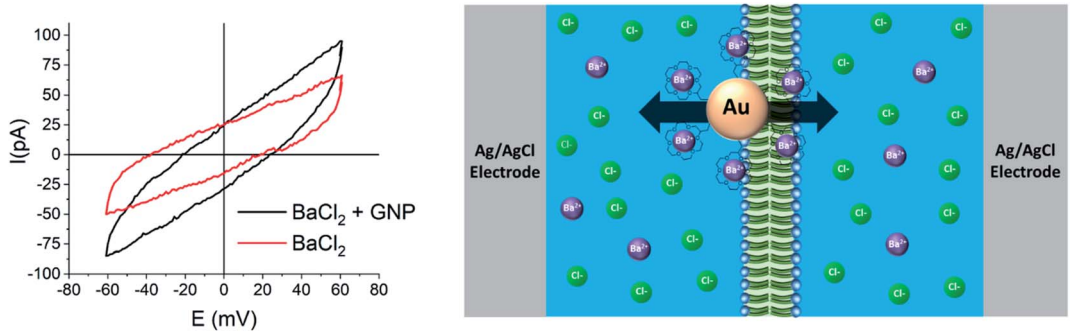

Fig. 2 Cyclic voltammetry of a phospholipid bilayer membrane separating two aqueous compartments both containing a 45 mM aqueous solution of $BaCl_2$ in the presence of barium-complexing GNPs (black line) and in their absence (red line). The near symmetric current increase in the presence of the GNPs indicates membrane transport of charged carrier particles as illustrated in the image. These experiments confirm the ability of the GNPs to mediate barium ion transfer across surfactant boundaries, either by crossing, or by flipping between the two sides of the membrane.

different droplet types many times to account for the amount of precipitate observed. Their ability to do this is further supported by the observation that a precipitate is formed in the *target* droplets regardless to which aqueous phase the GNPs had initially been added. Transport is likely to occur mainly across the surfactant boundary between adjacent water droplets, while GNPs that have transferred into the chloroform phase and diffused away from the emulsion can no longer participate in this process. Preliminary experiments with other highly insoluble systems such as silver chloride indicated difficulties to trap the reaction away from equilibrium since some reactants were able to partition between water and chloroform also in the absence of a specific transport mechanism. We have previously reported the transfer of a number of different GNPs across phospholipid mono- and bilayer membranes and also noted their ability to carry across ionic charge.[35–38] Drawing on this experience, we have conducted an electrochemical experiment that independently confirms barium ion transport across such a hydrophobic boundary between two aqueous compartments.

The cyclic voltammetry data presented in Fig. 2 show the effect of the presence of modified GNPs on barium ion transfer across an artificial phospholipid bilayer membrane separating two identical aqueous solutions of barium chloride. The significantly increased conductance of the membrane when crown ether modified GNPs are present confirms that they act as ion transporters. GNPs modified with different sized crowns act as membrane transporters for different ions including protons.[38] Crown ethers or GNPs alone do not show this effect. Here, the driving force is the externally applied potential across the membrane, while in the emulsion system it is the steep barium concentration gradient between *source* and *target* droplets, which is sustained by the precipitation of barium sulfate in the *target* droplets. We cannot rule out in either of the two systems that the transporter GNPs remain attached to the surfactant layer/membrane and flip between adjacent compartments rather than undergo full transfer. In the emulsion, continuous transfer of barium ions from *source* to *target* droplets cannot occur as the only process, since, unlike the electrochemical case, the charge separation associated with it has to be compensated internally to maintain electroneutrality of the system. A proposal of how this may happen is schematically illustrated in Fig. 3.

We suggest that this is achieved by concomitant transport of other cations from *target* to *source* droplets as the GNPs are going back and forth between different droplets. A range of different sulfates have been used in the *target* droplets without notably affecting the overall process (ESI3†). Cations that form no, or weak complexes, with the crown ether such as Li^+, K^+, Cs^+ or Mg^{2+}, can electrostatically replace the barium ions that have been removed from the ligand shell of the GNPs by precipitation.[34] Significant co-transport of anionic species to maintain electroneutrality is unlikely since this would lead to the precipitation of barium sulfate also in the *source* droplets (by gradual ingress of sulfate), which is not observed. A range of different barium salts (Cl^-, NO_3^-, ClO_4^- and acetate) had no noticeable effect on the overall process observed (Fig. ESI8†), and the potential role of anions has not been investigated further. For a detailed quantitative discussion of the complexation equilibria in both *source* and *target* droplets and their interplay with the electrostatic charging of the GNPs see section ESI4.† In principle, the charge separation associated with the unidirectional transport of barium ions could also remain uncompensated and lead instead to capacitive charging of the emulsion droplets. If we assume the formation of a small cube of barium sulfate of only 5 μm length, this would require the transport of approximately 2.5×10^{-12} moles of barium ions with a total charge of 5×10^{-7} As. In a typical emulsion droplet of 150 μm diameter and an interfacial capacitance of 1–10 μF cm^{-2} (high estimate) this would lead to an interfacial potential on the order of 100–1000 V, which is unrealistic since ion transport would be electrostatically impeded as soon as a potential of a few tens of millivolts is established. Simply treating the water droplet as a conducting sphere within a dielectric matrix of chloroform leads to yet higher estimates of electrostatic potential.[39,40] It can therefore be concluded that uncompensated transport of barium ions cannot account for the formation of the precipitates observed.

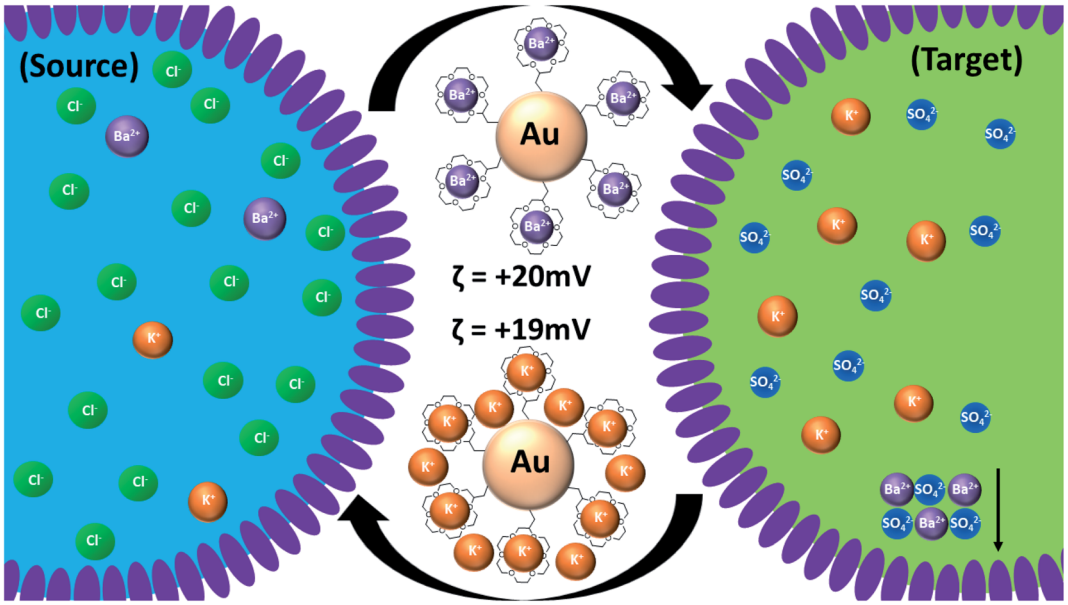

Fig. 3 Proposed mechanism of electroneutral transport of barium ions across the surfactant boundary from *source* to *target* droplets. Note that the replacement of barium ions may occur both by complexation and by electrostatic association of alternative cations (here potassium) within the ligand shell of the GNPs. The zeta-potential values given refer to separate measurements that emulate the conditions in the emulsion droplets (see text).

To understand better the role of GNP charge, measurements of the zeta potential of various aqueous dispersions of GNPs were conducted emulating the conditions that prevail within the emulsion droplets. In the absence of complexing ions, the zeta-potential of the as prepared GNPs is slightly negative, around −10 mV. Upon addition of just a small amount of $BaCl_2$ (1 mM) to simulate the environment of the *source* droplets, it increases to around 20 mV indicating strong complexation. After adding the same amount of K_2SO_4 (*target* droplet), as expected, barium sulfate precipitates. After removing the precipitate by centrifugation, the zeta-potential was still 19 mV, indicating that the exchange of Ba^{2+} with K^+ has no significant effect on the overall amount of charge residing on a particle. This supports the assumption that additional cations not directly complexed by the crown can also contribute to keeping the charge of the GNPs constant, as suggested in Fig. 3. It also supports our notion of how barium ion transport in this system is charge compensated. Notably, under the conditions of the emulsion experiments, the GNPs always carry a significant amount of net charge (positive zeta potential), which helps to retain them within the water droplet phase of the emulsion. In a separate experiment, using a two-phase water/chloroform system, it is shown that complexation of cations, which makes the crown-ether more hydrophobic,[34,35,41] causes the GNPs to partition between both phases and also to settle at the phase boundary (Fig. ESI11†). Such phase transfer is favored when their zeta potential is close to zero. As shown below, this reduces the amount of barium sulfate formed. Thus, the cations have two opposing effects, (I) complexation, making the GNPs more hydrophobic, and (II) charging, making them more hydrophilic.

The cation exchange in the ligand shell of the GNPs can, in principle, be accompanied by electron transfer to or from the metallic core of the GNPs. This is of interest since it may open opportunities of mechanistically coupling simple ionic charging processes with electron transfer reactions using the metal particle as an electron pool.[42] It is well established that even small GNPs (1.5 nm) can be charged by removal or addition of electrons.[43] Hence, electronic charging of 7 nm GNPs should readily proceed in the presence of a suitable redox couple, and it may be possible to either assist, or suppress the formation of barium sulfate depending on how the GNPs are charged. The results obtained for additions of the Fe(II)/Fe(III) redox couple in the form of the anionic complex potassium

Table 1 All possible combinations of Fe(II) and/or Fe(III) present as anionic hexacyanoferrate complex in the aqueous droplets, and resultant percentage of *target* droplets containing $BaSO_4$ precipitates. Std. deviation represents 3 repeats. Bold text represents samples with *higher* values than sample 1 (no redox additives), italic *lower*

Sample number	Additive in *source* droplet	Additive in *target* droplet	Proportion of *target* droplets in which $BaSO_4$ is visible
1	None	None	12 ± 3%
2	None	Fe(II)	**27 ± 3%**
3	None	Fe(III)	13 ± 4%
4	Fe(II)	None	*3 ± 4%*
5	Fe(II)	Fe(II)	16 ± 2%
6	Fe(II)	Fe(III)	*2 ± 2%*
7	Fe(III)	None	18 ± 3%
8	Fe(III)	Fe(II)	**48 ± 5%**
9	Fe(III)	Fe(III)	14 ± 3%

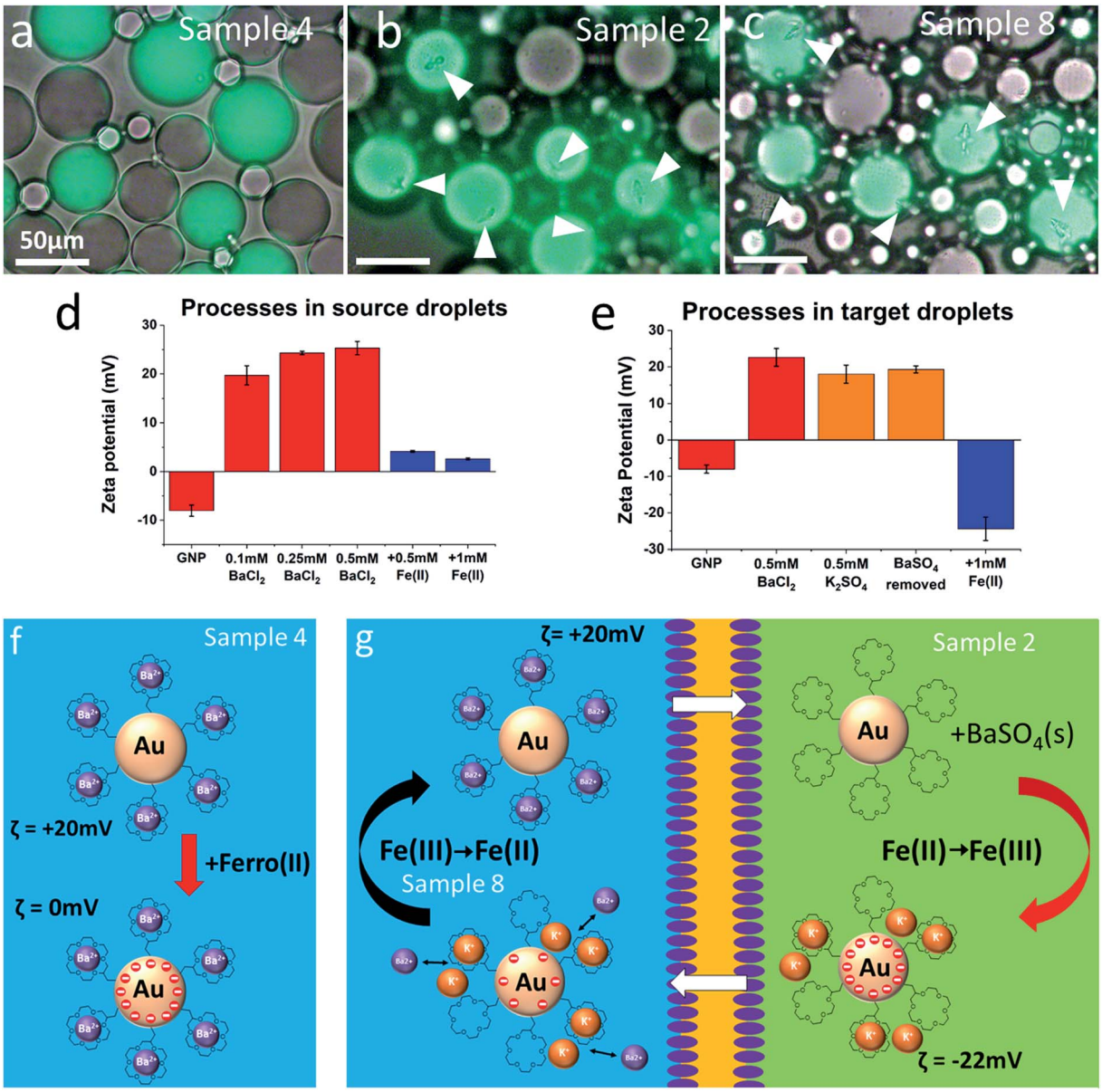

Fig. 4 Discussion of key results from Table 1. All microscope images were obtained after 10 minutes of mixing, and no further precipitation was observed. The presence of a redox couple influences the degree of barium ion transport by regulating the zeta-potential of the GNPs. Zeta potentials were separately determined in aqueous dispersions emulating the conditions of the *source* (d) and the *target* (e) droplets by sequential additions of salt (as indicated). Fe(II) in the *source* droplets leads to virtually uncharged particles (a and f) which reside preferentially in the chloroform phase and contribute less to the process. Hence, no or only very little, precipitation of barium sulfate is observed. Conversely, Fe(II) in the *target* droplets (b, g, sample 2) charges the particles negatively and reduces their tendency to escape into the chloroform phase. Finally, Fe(III) in the *source* droplets (c, g, sample 8) helps to remove negative electronic charge from the particles, which then become positively charged through exchange of potassium against barium ions and are therefore again prevented from escaping into the chloroform phase.

ferro/ferri cyanide, are summarized in Table 1. All microscope images were obtained after 10 minutes of mixing when no further change was observed.

It is evident that the presence of the redox couple has an effect on the formation of barium sulfate, but the correlations found cannot be explained straightforwardly by assuming that the electronic charging of the metal cores facilitates the exchange of ionic charge in the ligand shell. In fact, the trends observed are opposite of what would be expected if this were the case. For example, the presence of Fe(II) in the *source* droplets and Fe(III) in the *target* droplets (sample 6) should facilitate barium ion transport by maintaining electroneutrality in both droplet types through coupled electron transfer. Instead, barium sulfate formation is almost completely suppressed. There is thus no indication that coupled electron transfer assists the ion exchange processes in any way. Instead, it appears to be the interplay between net charge and hydrophobicity of the GNPs that moderates their ability to transport

barium ions from *source* to *target* droplets as illustrated in Fig. 4.

The complexing of the ligand shell with barium ions in the *source* droplets has two opposing effects. As mentioned before, it increases the hydrophobicity of the crown ether ligand,[34,35,41] but it also increases the net charge of the GNPs making them more dispersible in water. The presence of Fe(II) (samples 4, 5 and 6) can bring down the zeta potential of the particles close to zero (Fig. 4d) by electron transfer from the iron complex to the metallic GNP core and can result in less formation of barium sulfate precipitate (samples 4 and 6). This may be related to a charge-regulated change in the partitioning of GNPs between chloroform and water. On the other hand, in the *target* droplets, along with loss of barium ions and partial complexation of potassium ions, Fe(II) charges the particles negatively (Fig. 4e) by electron transfer, which helps the retention of the GNPs within the aqueous part of the emulsion (samples 2 and 8). It also enhances the electrostatic association of cations (*e.g.* K^+) with the GNPs, which assists the maintenance of electroneutrality of the emulsion (see Fig. 4g). Fe(III) in general appears to play a less significant role. Its presence in the *source* droplets seems to assist positive charging of the particles and thereby helps to prevent the irreversible loss of particles into the chloroform. Unfortunately, zeta potential measurements in the presence of Fe(III) were impeded by GNP aggregation under these conditions.

Generally, zeta potentials close to zero seem to suppress the formation of barium sulfate, while positive and negative values significantly away from zero enhance it. These observations support the notion that the GNPs predominantly shuttle the barium ions across the surfactant boundaries between two contacting water droplets, while near charge neutral, more hydrophobic GNPs are washed out into the chloroform phase and appear to be lost for this process.

Experimental section/methods

Gold nanoparticle synthesis

Tri-sodium citrate, potassium carbonate, tannic acid, $HAuCl_4$, KCl, NaCl and LiCl were all used as purchased from Sigma Aldrich. 18-Crown-6-CH_2-SH was used as purchased from Pro-Chimia. Details of gold nanoparticle (GNP) synthesis can be found in our previous publication.[34] In short, monodisperse GNPs were prepared using a modified citrate reduction method with the addition of tannic-acid,[44] resulting in particles with high stability in aqueous media.

Synthesis of 4 nm Au seeds

Potassium carbonate (150 mM, 1 ml) and tannic acid (2.5 mM, 0.1 ml) were added to an aqueous solution of tri-sodium citrate (2.2 mM, 150 ml) and heated to 70 °C under vigorous stirring. Then, tetrachloroauric acid ($HAuCl_4$) (25 mM, 1 ml) was rapidly injected under vigorous stirring. The reaction mixture immediately darkened and gradually turned clear and light orange over a period of 10 min, indicating the formation of well dispersed Au seeds.

Growth of seeds to 7 nm GNPs

15 minutes after the injection of $HAuCl_4$, 55 ml of the seed solution was removed. To the remainder, tri-sodium citrate (2.2 mM, 55 ml) was added under vigorous stirring and heated again to 70 °C. Then, $HAuCl_4$ (25 mM, 0.5 ml) was rapidly injected under vigorous stirring. The mixture initially turned purple and then gradually changed to orange/red. After 15 minutes a second injection of $HAuCl_4$ (25 mM, 0.5 ml) was carried out under vigorous stirring, and the solution was again left for 15 minutes. This step was repeated once more to yield the desired size of 7 nm confirmed by TEM and DLS.

The particles were coated with thiolated crown ether (18-crown-6-CH_2-SH) followed by the removal of excess ligand and salts by repeated centrifugation (14 600 rpm, 60 min, 3 °C and 13 000 rpm, 60 min, 3 °C). PEG stabilized control particles were prepared as reported earlier.[45]

Emulsion preparation

All samples were prepared by gently combining two emulsions, one containing the *source* and the other the *target* droplets. Both were water-in-chloroform emulsions, each prepared in a 1 to 4 ratio and stabilized by the surfactant Span80 (2% w/w in $CHCl_3$). Emulsification was carried out by vigorous shaking, typically after pipetting 100 μl of the aqueous solution to 400 μl of the chloroform phase. The concentration of each salt ($BaCl_2$, K_2SO_4, $K_4[Fe(CN)_6]$ and $K_3[Fe(CN)_6]$) present in the aqueous phase was 25 mM. The sulfate-containing droplets also contained 1 mM calcein as a fluorescent label, which is not soluble in the organic phase. For all experiments involving GNPs, an initial concentration of 17 nM (in the water droplets) was used.

Zeta-potential measurements

Zeta-potentials were measured with a Malvern Zetasizer (NANO ZSP). Samples were prepared in Eppendorf tubes (volume 0.5 ml) and transferred for measurement to a disposable capillary-cell (DTS1070). The temperature was set to 25 °C and samples were allowed to equilibrate for 5 minutes. Standard deviation values are based on five measurements.

Optical microscopy

To prevent the evaporation of the chloroform phase, emulsion samples (100 μl) were placed on cavity soda-lime glass slides protected by glass cover slips. A Brunel SP300F microscope equipped with a CCD camera (UCMOS 5100 KPA) and a Hg-arc lamp for fluorescence excitation was used. For consistency between different samples, all optical (white light intensity and filters) and digital (camera integration time, gain and temperature adjustment) parameters were kept constant. A pinhole was used to adjust the amount of white light needed for the appropriate illumination at different magnifications. Results presented in Table 1 are based on analyzing at least 20 representative images of each sample, each containing between 50 and 100 droplets, with 2 repeat measurements of each sample. This was done by manually counting the calcein-labelled *target*

droplets and detecting the presence of $BaSO_4$ precipitates using ImageJ software.

Raman microscopy

Samples (100 μl) were inspected on cavity soda-lime glass slides under glass cover-slips. Raman spectra were recorded with a Renishaw inVia Confocal Raman microscope with excitation wavelength of 532 nm at 100% power and 50× objective lens. The baseline of each spectrum was corrected using WiRE 4.4 software (Renishaw). $BaSO_4$ peaks were identified from literature.[46]

Electron microscopy

Samples were inspected with an environmental SEM (FEI Quanta 250) capable of operating under fully hydrated conditions. By controlling the water vapor pressure (up to 2700 Pa) in the chamber and the sample holder temperature (from −20 °C to 60 °C), the relative humidity around the sample can be set in the range from 0 to 100%. For cryo-SEM, 5 μl emulsion samples were shock-frozen by dripping them directly into liquid nitrogen. The solid samples were collected, quickly placed on the pre-cooled ESEM sample holder (set to −15 °C) and gently crushed using a pair of tweezers (Fig. ESI12†). At this temperature, the continuous chloroform phase rapidly evaporates, but the aqueous emulsion droplets remain frozen and can be examined in the ESEM in low-vacuum mode. By keeping the chamber pressure at around 200 Pa, the relative humidity was maintained just below 100% so that individual droplets could be imaged for up to 20 minutes before they would have sublimed completely. Note that successful imaging requires fine tuning of the ESEM conditions. When the humidity is too high, ice crystals form on the sample surface (Fig. ESI12†). On the other hand, when it is too low, the frozen water droplets sublime too quickly, and their structural integrity is compromised (Fig. ESI12†). The exact imaging conditions vary slightly from sample to sample as they all have slightly different shapes and thermal contact with the cooled sample holder.

Cyclic voltammetry

The electrochemical set-up for charge transport measurements across phospholipid bilayer membranes was constructed following the methods described by Tsofina *et al.*[47] and Bayley *et al.*[48] Briefly, a 3D-printed cell equipped with an Ag/AgCl electrode was filled with electrolyte solution (45 mM $BaCl_2$ in Milli-Q water, 300 μl). Then, 100 μl of a solution of the phospholipid asolectin in decane (25 mg ml^{-1}) was pipetted on top of it to form an interfacial monolayer. A droplet (3.5 μl) of electrolyte was then suspended on a further Ag/AgCl electrode coated with an agarose electrolyte gel, and slowly lowered with a micro-manipulator through the decane layer, until the two monolayers formed at each boundary between the aqueous and organic phases contacted to create a bilayer membrane. The area of this membrane was approximately 2.8×10^{-2} cm^2. Membrane conductance and capacitance were measured by cyclic voltammetry.

The membrane capacitances measured were approximately 10 nF, which corresponds to 0.36 μF cm^{-2}. This compares very well with literature values.[49] Adding the 7 nm (166 nM) 18-crown-6-functionalised GNPs on both sides of the membrane doubled the electrical conductivity (from 2.2×10^{-8} S cm^{-2} to 4.4×10^{-8} S cm^{-2}). At 60 mV and −60 mV, the currents generated after adding the particles were 29 pA and 35 pA, respectively. We attribute this slight asymmetry to deviations of the non-polarizable Ag/AgCl electrodes from ideal behaviors. These currents correspond to an ion transfer rate across the membrane of 3.6×10^8 and 4.4×10^8 Ba^{2+} ions per s, respectively. This order of magnitude of ionic transport is realistic when assuming that each GNP carries 10 to 100 ions across the membrane each second, which would require that about 10^6 to 10^7 GNPs are involved in this process. These particles would take up a total area that is roughly four orders of magnitude smaller than that of the membrane and could therefore easily be accommodated at any time without compromising the membrane's structural identity.

Conclusion

We have shown that segregation of ionic reactants by microscale compartmentalization in emulsion droplets can arrest a simple chemical process away from equilibrium. The addition of a nanoscale shuttle, independently tested by electrochemical membrane transport, unlocks the system by bringing the reactants together. Our main focus here has been on directional ion transport from droplets containing barium ions to those containing sulfate. The resulting precipitation of highly insoluble barium sulfate in the *target* droplets is the overall driving force of the transport process. Electroneutrality demands the presence of secondary processes that compensate for the charge separation associated with ion transport. These have not yet been identified and could involve ion exchange as well as electron transfer reactions. Charging the metal cores by an added redox couple has been shown to influence the effectivity of the GNPs as ion transporters within the emulsion by regulating the partitioning of the particles between the water and chloroform phases. We suggest that direct transfer of GNPs between adjacent droplets is the predominant transport mechanism, while GNPs once dispersed in the chloroform phase may be washed out and no longer contribute. Future improvements of our system will aim to create emulsions with no excess continuous phase, so that the GNPs cannot diffuse away from the water droplets and potentially remain amenable as ion transporters.

Author contributions

Conceptualization: M. Brust, C. Kunstmann-Olsen; Resources: M. Brust, Y. A. Diaz Fernandez, R. Raval; Data curation: C. Kunstmann-Olsen, D. Belic, S. P. Danks, D. F. Bradley, X. Qiao, A. P. Hill, I. Sorzabal-Bellido; Formal analysis: C. Kunstmann-Olsen, M. Brust, D. Belic, D. F. Bradley, S. P. Danks, Y. A. Diaz Fernandez, M. P. Grzelczak, A. P. Hill, X. Qiao, I. Sorzabal-Bellido; Supervision: M. Brust, C. Kunstmann-Olsen, Y. A. Diaz Fernandez; Funding acquisition: M. Brust, R. Raval;

Investigation; C. Kunstmann-Olsen, D. Belic, M. P. Grzelczak, A. P. Hill, X. Qiao, I. Sorzabal-Bellido; Visualization; C. Kunstmann-Olsen, X. Qiao; Methodology: C. Kunstmann-Olsen, M. Brust, D. Belic, D. F. Bradley, S. P. Danks, Y. A. Diaz Fernandez, M. P. Grzelczak; Writing—original draft: C. Kunstmann-Olsen, M. Brust, Y. A. Diaz Fernandez, S. P. Danks; Writing—review and editing: C. Kunstmann-Olsen, M. Brust. All authors have read and agreed to the published version of the manuscript.

Conflicts of interest

There are no conflicts to declare.

Acknowledgements

This research was funded by the European Research Council via ERC-Advanced Grant 321172, PANDORA (MB). AH and SPD were supported by EPSRC PhD studentships and XQ by the University of Liverpool. In addition, RR, YDF and ISB acknowledge support by the Biotechnology and Biological Sciences Research Council (Award Number BB/R012415/1) and by the National Biofilms Innovation Centre (NBIC) which is an Innovation and Knowledge Centre funded by the Biotechnology and Biological Sciences Research Council, Innovate UK and Hartree Centre.

References

1 N. Koumura, R. W. J. Zijlstra, R. A. van Delden, N. Harada and B. L. Feringa, Light-driven monodirectional molecular rotor, *Nature*, 1999, **401**, 152.
2 V. Balzani, A. Credi, S. J. Langford, F. M. Raymo, J. F. Stoddart and M. Venturi, Constructing Molecular Machinery: A Chemically-Switchable [2]Catenane, *Angew. Chem., Int. Ed.*, 2000, **39**, 3348.
3 *Molecular machines and motors*, ed. J. P Sauvage, Springer Science, 2001.
4 R. A. van Delden, M. K. J. ter Wiel, M. M. Pollard, J. Vicario, N. Koumura and B. L. Feringa, Unidirectional molecular motor on a gold surface, *Nature*, 2005, **437**, 1337.
5 S. P. Fletcher, F. Dumur, M. M. Pollard and B. L. Feringa, A Reversible, Unidirectional Molecular Rotary Motor Driven by Chemical Energy, *Science*, 2005, **310**(5745), 80.
6 W. R. Browne and B. L. Feringa, Making molecular machines work, *Nat. Nanotechnol.*, 2006, **1**, 25.
7 M. Asakawa, P. R. Ashton, V. Balzani, A. Credi, G. Mattersteig, O. A. Matthews, M. Montalti, N. Spencer, J. F. Stoddart and M. Venturi, Electrochemically Induced Molecular Motions in Pseudorotaxanes: A Case of Dual-Mode (Oxidative and Reductive) Dethreading, *Chem. - Eur. J.*, 2006, **12**, 1992.
8 R. Eelkema, M. M. Pollard, J. Vicario, N. Katsonis, B. S. Ramon, C. W. M. Bastiaansen, D. J. Broer and B. L. Feringa, Nanomotor rotates microscale objects, *Nature*, 2006, **440**, 163.
9 E. R. Kay, D. A. Leigh and F. Zerbetto, Synthetic molecular motors and mechanical machines, *Angew. Chem., Int. Ed.*, 2007, **46**, 72.
10 S. Erbas-Cakmak, D. A. Leigh, C. T. McTernan and A. L. Nussbaumer, Artificial Molecular Machines, *Chem. Rev.*, 2015, **115**, 10081.
11 C. Cheng, P. R. McGonigal, J. F. Stoddart and R. D. Astumian, Design and Synthesis of Nonequilibrium Systems, *ACS Nano*, 2015, **9**(9), 8672.
12 M. R. Wilson, J. Solà, A. Carlone, S. M. Goldup, N. Lebrasseur and D. A. Leigh, An autonomous chemically fuelled small-molecule motor, *Nature*, 2016, **534**, 235.
13 H. Logtenberg, J. Areephong, J. Bauer, A. Meetsma, B. L. Feringa and W. R. Browne, Towards Redox-Driven Unidirectional Molecular Motion, *ChemPhysChem*, 2016, **17**, 1895.
14 B. Collins, J. Kistemaker, E. Otten and B. L. Feringa, A chemically powered unidirectional rotary molecular motor based on a palladium redox cycle, *Nat. Chem.*, 2016, **8**, 860.
15 S. Erbas-Cakmak, S. D. P. Fielden, U. Karaca, D. A. Leigh, C. T. McTernan, D. J. Tetlow and M. R. Wilson, Rotary and linear molecular motors driven by pulses of a chemical fuel, *Science*, 2017, **358**, 340.
16 L. Zhang, V. Marcos and D. A. Leigh, Molecular machines with bio-inspired mechanisms, *Proc. Natl. Acad. Sci. U. S. A.*, 2018, **115**(38), 9397.
17 S. Mann, The Chemistry of Form, *Angew. Chem., Int. Ed.*, 2000, **39**, 3392.
18 M. Li and S. Mann, Emergence of Morphological Complexity in BaSO4 Fibers Synthesized in AOT Microemulsions, *Langmuir*, 2000, **16**(17), 7088.
19 S. Mann, Systems of Creation: The Emergence of Life from Nonliving Matter, *Acc. Chem. Res.*, 2012, **45**(12), 2131.
20 G. Piedrafita, K. Ruiz-Mirazo, P.-A. Monnard, A. Cornish-Bowden and F. Montero, Viability Conditions for a Compartmentalized Protometabolic System: A Semi-Empirical Approach, *Plos One*, 2012, **7**(6), e39480.
21 P.-A. Monnard and P. Walde, Current Ideas about Prebiological Compartmentalization, *Life*, 2015, **5**(2), 1239.
22 L. Wang, P. Wen, X. Liu, Y. Zhou, M. Li, Y. Huang, L. Geng, S. Mann and X. Huang, Single-step fabrication of multi-compartmentalized biphasic proteinosomes, *Chem. Com.*, 2017, **53**(61), 8537.
23 P. A. Beales, B. Ciani and S. Mann, The artificial cell: biology-inspired compartmentalization of chemical function, *Interface Focus*, 2018, **8**, 20180046.
24 M. Kirch and J. -M. Lehn, Selective Transport of Alkali Metal Cations through a Liquid Membrane by Macrobicyclic Carriers, *Angew. Chem., Int. Ed.*, 1975, **14**(8), 555.
25 M. Capdevila, A. Maestro, M. Porras and J. M Gutiérrez, Preparation of Span 80/oil/water highly concentrated emulsions: Influence of composition and formation variables and scale-up, *J. Colloid Interface Sci.*, 2010, **345**(1), 27.
26 P. Gruner, B. Riechers, B. Semin, J. Lim, A. Johnston, K. Short and J.-C. Baret, Controlling molecular transport in minimal emulsions, *Nat. Commun.*, 2016, **7**, 10392.
27 Y. Chen, A. W. Gani and S. K. Y. Tang, Characterization of sensitivity and specificity in leaky droplet-based assays, *Lab Chip*, 2012, **12**, 5093.

28 H. Kuang, W. Chen, W. Yan, L. Xu, Y. Zhu, L. Liu, H. Chu, C. Peng, L. Wang, N. A. Kotov and C. Xu, Crown ether assembly of gold nanoparticles: melamine sensor, *Biosens. Bioelectron.*, 2011, **26**, 2032.

29 A. C. Templeton, M. J. Hostetler, E. K. Warmoth, S. Chen, C. M. Hartshorn, V. M. Krishnamurthy, M. D. E. Forbes and R. W. Murray, Gateway Reactions to Diverse, Polyfunctional Monolayer-Protected Gold Clusters, *J. Am. Chem. Soc.*, 1998, **120**(19), 4845.

30 S. Y. Lin, S.-W. Liu, C.-M. Lin and C. h Chen, Recognition of Potassium Ion in Water by 15-Crown-5 Functionalized Gold Nanoparticles, *Anal. Chem.*, 2002, **74**(2), 330.

31 K. Y. Lee, Y. Bae, M. Kim, G.-W. Cheong, J. Kim, S. S. Lee and S. W. Han, Crown ether derivatives-mediated self-assembly of nanoparticles at the liquid/liquid interface, *Thin Solid Films*, 2006, **515**(4), 2049.

32 M. I. Bodnarchuk, S. Yakunin, L. Piveteau and M. V. Kovalenko, Host–guest chemistry for tuning colloidal solubility, self-organization and photoconductivity of inorganic-capped nanocrystals, *Nat. Com.*, 2015, **6**, 10142.

33 F. Dumur, E. Dumas and C. R. Mayer, Functionalization of Gold Nanoparticles by Inorganic Entities, *Nanomaterials*, 2020, **10**(3), 548.

34 A. P. Hill, C. Kunstmann-Olsen, M. P. Grzelczak and M. Brust, Entropy-Driven Reversible Agglomeration of Crown Ether Capped Gold Nanoparticles, *Chem. –Eur. J.*, 2018, **24**, 3151.

35 M. P. Grzelczak, A. P. Hill, D. Belic, D. F. Bradley, C. Kunstmann-Olsen and M. Brust, Design of artificial membrane transporters from gold nanoparticles with controllable hydrophobicity, *Faraday Discuss.*, 2016, **191**, 495.

36 G. J. Gordillo, Z. Krpetic and M. Brust, Interactions of Gold Nanoparticles with a Phospholipid Monolayer Membrane on Mercury, *ACS Nano*, 2014, **8**, 6074.

37 M. P. Grzelczak, S. P. Danks, R. C. Klipp, D. Belic, A. Zaulet, C. Kunstmann-Olsen, D. F. Bradley, T. Tsukuda, C. Vinas, F. Teixidor, J. J. Abramson and M. Brust, Ion Transport across Biological Membranes by Carborane-Capped Gold Nanoparticles, *ACS Nano*, 2017, **12**, 12492.

38 S. P. Danks, PhD thesis, University of Liverpool, 2020.

39 Y.-M. Jung, H.-C. Oh and I. S. Kang, Electrical charging of a conducting water droplet in a dielectric fluid on the electrode surface, *J. Colloid Interface Sci.*, 2008, **322**(2), 617.

40 D. J. Im, M. M. Ahn, B. S. Yoo, D. Moon, D. W. Lee and I. S. Kang, Discrete Electrostatic Charge Transfer by the Electrophoresis of a Charged Droplet in a Dielectric Liquid, *Langmuir*, 2012, **28**(32), 11656.

41 D. J. Sam and H. E. Simmons, Crown Polyether Chemistry. Potassium Permanganate Oxidations in Benzene, *J. Am. Chem. Soc.*, 1972, **94**(11), 4024.

42 A. M. Cioran, A. D. Musteti, F. Teixidor, Ž. Krpetić, I. A. Prior, Q. He, C. J. Kiely, M. Brust and C. Viñas, Mercaptocarborane-Capped Gold Nanoparticles: Electron Pools and Ion Traps with Switchable Hydrophilicity, *J. Am. Chem. Soc.*, 2012, **134**(1), 212.

43 R. W. Murray, Nanoelectrochemistry: Metal Nanoparticles, Nanoelectrodes, and Nanopores, *Chem. Rev.*, 2008, **108**, 2688.

44 J. Piella, N. G. Bastus and V. Puntes, Size-Controlled Synthesis of Sub-10-nanometer Citrate-Stabilized Gold Nanoparticles and Related Optical Properties, *Chem. Mater.*, 2016, **4**, 1066.

45 C. Kunstmann-Olsen, D. Belić, D. F. Bradley, M. P. Grzelczak and M. Brust, Humidity-Dependent Reversible Transitions in Gold Nanoparticle Superlattices, *Chem. Mater.*, 2016, **28**(9), 2970.

46 J. D. Gelder, P. Vandenabeele, F. Govaert and L. Moens, Forensic analysis of automotive paints by Raman spectroscopy, *J. Raman Spectrosc.*, 2005, **36**, 1059.

47 L. M. Tsofina, E. A. Liberman and A. V. Babakov, Production of Bimolecular Protein-Lipid Membranes in Aqueous Solution, *Nature*, 1966, **212**, 681.

48 H. Bayley, B. Cronin, A. Heron, M. A. Holden, W. L. Hwang, R. Syeda, J. Thompson and M. Wallace, Droplet interface bilayers, *Mol. Biosyst.*, 2008, **3**, 1191.

49 S. H. White and T. E. Thompson, Capacitance, area, and thickness variations in thin lipid films, *Biochim. Biophys. Acta*, 1973, **323**, 7.